Available online at www.sciencedirect.com
ScienceDirect
Physica D 237 (2008) 2411–2422
PHYSICA D
www.elsevier.com/locate/physd

A universal separatrix map for weak interactions of solitary waves in generalized nonlinear Schrödinger equations

Yi Zhu[a], Richard Haberman[b], Jianke Yang[c,*]

[a] Zhou Pei-Yuan Center for Applied Mathematics, Tsinghua University, Beijing 100084, China
[b] Department of Mathematics, Southern Methodist University, Dallas, TX 75275, USA
[c] Department of Mathematics and Statistics, University of Vermont, Burlington, VT 05401, USA

Received 30 November 2007; received in revised form 7 March 2008; accepted 19 March 2008
Available online 27 March 2008

Communicated by K. Promislow

Abstract

It is known that weak interactions of two solitary waves in generalized nonlinear Schrödinger (NLS) equations exhibit fractal dependence on initial conditions, and the dynamics of these interactions is governed by a universal two-degree-of-freedom ODE system [Y. Zhu J. Yang, Universal fractal structures in the weak interaction of solitary waves in generalized nonlinear Schrödinger equations, Phys. Rev. E 75 (2007) 036605]. In this paper, this ODE system is analyzed comprehensively. Using asymptotic methods along separatrix orbits, a simple second-order map is derived. This map does not have any free parameters after variable rescalings, and thus is universal for all weak interactions of solitary waves in generalized NLS equations. Comparison between this map's predictions and direct simulations of the ODE system shows that the map can capture the fractal-scattering phenomenon of the ODE system very well both qualitatively and quantitatively.

PACS: 42.65.Tg; 05.45.Yv; 42.81.Dp

Keywords: Weak interactions; Solitary waves; Fractal scattering; Separatrix map

1. Introduction

Interactions of solitary waves in nonlinear wave equations are a fascinating mathematical phenomena, and they also arise in numerous physical and engineering applications [1,2]. Strong interactions, often called collisions, occur when two solitary waves are initially far apart but move toward each other at moderate or large speeds. Weak interactions would occur if the two waves are initially well separated, and their relative velocities are small or zero. If the wave equations are integrable, strong interactions of solitary waves are elastic [1], and their weak interactions exhibit interesting but simple behaviors [2–5]. For certain integrable systems with higher-order corrections, if they can be asymptotically transformed to integrable equations, then their solitary wave interactions would closely resemble those in integrable systems [6–8]. On the other hand, in some non-integrable equations, solitary wave interactions are extremely complicated, and they can depend on initial conditions (such as velocities or phases) in a very sensitive, fractal manner. This fractal-scattering phenomenon was discovered first for kink-antikink collisions in the ϕ^4 model [9–14] and later in several other physical systems as well [15–20]. For these strong interactions, a resonant energy exchange mechanism between the collision and internal/radiation modes was found responsible for this chaotic scattering. For weak interactions, fractal scattering has been found as well in several wave systems [21–23].

Intrigued by these fractal scattering phenomena, the mathematical analysis ensued. For strong interactions, approximate collective-coordinate ODE models based on variational methods were first derived, and they were found to exhibit qualitatively similar fractal scattering as in the PDEs [14,16,24,20]. To further the mathematical analysis, Goodman and Haberman studied these collective-coordinate ODE models using

* Corresponding author.
E-mail addresses: zhuyi03@mails.tsinghua.edu.cn (Y. Zhu), rhaberma@mail.smu.edu (R. Haberman), jyang@cems.uvm.edu (J. Yang).

0167-2789/$ - see front matter © 2008 Elsevier B.V. All rights reserved.
doi:10.1016/j.physd.2008.03.030

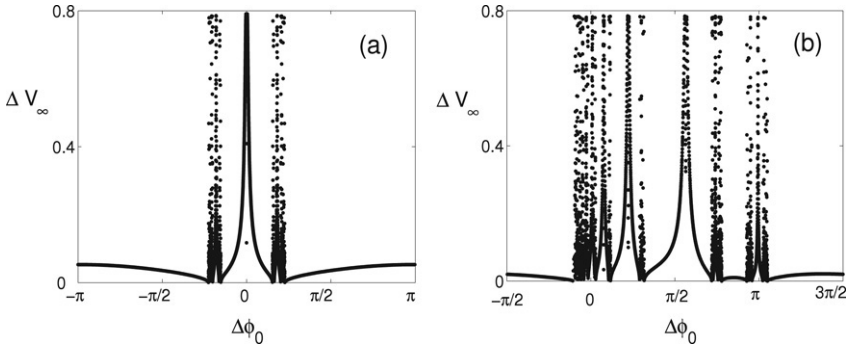

Fig. 2.1. Exit velocity (ΔV_∞) versus the initial phase difference ($\Delta\phi_0$) graphs in the PDE (2.1) with nonlinearity (2.3); (a, b) are for initial conditions (2.4) and (2.5) respectively (after [23]).

sophisticated dynamical systems methods [25–28]. Performing asymptotic analysis along separatrix (homoclinic) orbits, they derived separatrix maps which lead to the prediction of n-bounce resonance windows. For weak interactions, the mathematical analysis can be made more rigorous. Unlike the collective-coordinate ODE models for strong interactions which were approximate and PDE-dependent, Zhu and Yang derived a simple and asymptotically accurate ODE model for weak interactions in generalized NLS equations with arbitrary nonlinearities [23]. Due to the simplicity and universality of this ODE model, its rigorous mathematical analysis is highly desirable. However, this ODE model is quite different from the collective-coordinate ODE models studied in [25–28], and it has not been analyzed yet.

In this paper, we develop a comprehensive mathematical analysis for this universal ODE model for weak interactions of solitary waves. Our main result is the asymptotic derivation of the following simple second-order map near separatrix orbits

$$\mathcal{M}_{n+1} = \mathcal{M}_n - \frac{\operatorname{sgn}(\varepsilon \mathcal{Q}_n)}{\mathcal{Q}_n^2}, \tag{1.1}$$

$$\mathcal{Q}_{n+1} = \mathcal{Q}_n + 2\mathcal{M}_{n+1}, \tag{1.2}$$

where $\mathcal{M}_n$ is the (scaled) momentum of the ODE system at subsequent saddle approach points, $\mathcal{Q}_n$ is an auxiliary variable whose role will be made clear later, and ε is a perturbation parameter in the ODE system. This map does not have any free parameters, and thus is universal for all weak solitary-wave interactions in the generalized NLS equations. Comparison between this map's predictions and direct simulations of the ODE system shows that this map captures all the fractal-scattering phenomenon of the ODE system very well both qualitatively and quantitatively. Thus this map is a very valuable and reliable tool for the understanding of fractal scattering in weak solitary wave interactions.

A brief derivation of the separatrix map (1.1)–(1.2) was presented in [29]. The full analysis is detailed in this article.

2. Preliminaries and earlier works

In a previous paper [23], weak interactions in the generalized NLS equation

$$iU_t + U_{xx} + N(|U|^2)U = 0 \tag{2.1}$$

were studied. This equation admits solitary waves of the form

$$U = \Phi(x-\xi)e^{i\phi}, \tag{2.2}$$

where $\Phi(\theta)$ is a localized positive function, $\xi = Vt + x_0$ is the wave's center position, and $\phi = \frac{1}{2}V(x-\xi) + (\beta + \frac{1}{4}V^2)t - \eta_0$ is the wave's phase. This wave has four free parameters: velocity V, amplitude β, initial position x_0, and initial phase η_0. For weak interactions, two such solitary waves are initially well separated with small relative velocities and amplitude differences. They interfere with each other through tail overlapping. When time goes to infinity, they either separate from each other with constant velocities or form a bound state. The exit velocity, defined as $\Delta V_\infty = |V_2 - V_1|_{t\to\infty}$, depends on the initial conditions of the two waves. When the two waves form a bound state, $\Delta V_\infty = 0$. In [23], it was shown that, for a large class of nonlinearities $N(|U|^2)$, this weak interaction depends on the initial conditions in a sensitive fractal manner. An example is shown in Fig. 2.1. In this example, the nonlinearity is

$$N(|U|^2) = \alpha|U|^2 + \delta|U|^4, \tag{2.3}$$

with $\alpha = 1, \delta = 0.04$. For two sets of initial conditions (equal and unequal initial amplitudes respectively)

$$\begin{aligned} &x_{0,1} = -x_{0,2} = -5, \qquad V_{0,1} = V_{0,2} = 0,\\ &\beta_{0,1} = \beta_{0,2} = 1, \qquad \phi_{0,1} = 0, \end{aligned} \tag{2.4}$$

and

$$\begin{aligned} &x_{0,1} = -x_{0,2} = -5, \qquad V_{0,1} = V_{0,2} = 0,\\ &\beta_{0,1} = 1.0325, \qquad \beta_{0,2} = 0.9675, \qquad \phi_{0,1} = 0, \end{aligned} \tag{2.5}$$

both with the initial phase difference $\Delta\phi_0 = \phi_{0,2} - \phi_{0,1}$ as the control parameter, the exit velocity ΔV_∞ versus $\Delta\phi_0$ graphs are plotted in Fig. 2.1. These graphs are fractals (see [23] for details). To analyze this phenomenon, the Karpman–Solov'ev method [3] was applied (see also [4]), and the following simple set of dynamical equations for soliton parameters were derived [23]:

$$\begin{cases} \zeta_{\tau\tau} = \cos\psi e^{\zeta}, \\ \psi_{\tau\tau} = (1+\varepsilon)\sin\psi e^{\zeta}. \end{cases} \tag{2.6}$$

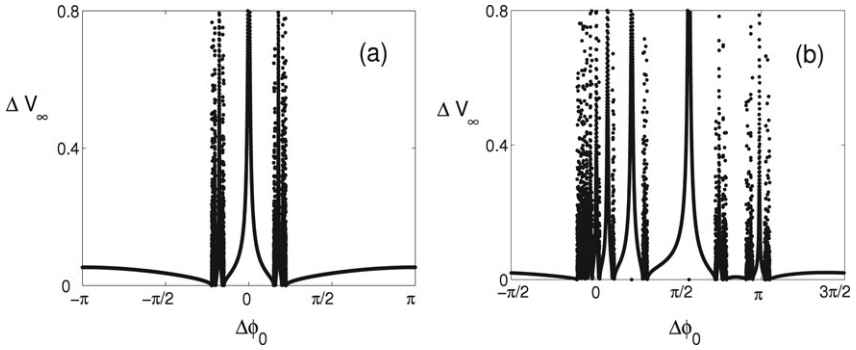

Fig. 2.2. Exit velocity (ΔV_∞) versus the initial phase difference ($\Delta\phi_0$) graphs obtained from the reduced ODEs (2.6); (a, b) correspond to Fig. 2.1(a, b) respectively (after [23]).

Here

$$\psi = \Delta\phi, \quad \zeta = -\sqrt{\beta}\Delta\xi, \\ \tau = \sqrt{\frac{16\beta^{3/2}c^2}{P}}t, \quad \varepsilon = \frac{P}{2\beta P_\beta} - 1, \tag{2.7}$$

$\Delta\xi$ and $\Delta\phi$ are the distance and phase difference between the two waves, $\beta = (\beta_{1,0} + \beta_{2,0})/2$, c is the tail coefficient of the solitary wave with propagation constant β, and $P(\beta)$ is the power function of the wave. Note that for the integrable cubic NLS equation where $N(|U|^2) = |U|^2$, $P(\beta) = 4\sqrt{\beta}$, and thus $\varepsilon = 0$. This reproduces the results in [3,4] as a special case.

Utilizing these reduced equations, we can predict the ΔV_∞ versus $\Delta\phi_0$ graphs for initial conditions (2.4) and (2.5), which correspond to

$$\zeta_0 = -10, \qquad \dot\zeta_0 = \dot\psi_0 = 0, \tag{2.8}$$

and

$$\zeta_0 = -10, \qquad \dot\zeta_0 = 0, \qquad \dot\psi_0 = -0.01167, \tag{2.9}$$

with $\varepsilon = 0.13665$ for (2.6) (see [23]). The results are displayed in Fig. 2.2. These graphs are also fractals [23]. Comparing them with the original Fig. 2.1 from PDE simulations, we see that they agree very well. Thus, the reduced ODEs (2.6) completely capture the fractal scattering dynamics of the PDEs both qualitatively and quantitatively. Because of this, the study of fractal scattering in the PDEs (2.1) can then be reduced to the study of the ODEs (2.6).

The ODEs (2.6) are a very interesting new dynamical system. It is universal (for the generalized NLS equations with arbitrary nonlinearities) and simple-looking, yet its dynamics are extremely rich. In [23], some basic properties of these ODEs were analyzed. It was observed that fractal structures bifurcate from singularity points of the system (2.6) with $\varepsilon = 0$. Conditions for the appearance of fractal structures were also stipulated from numerical observations. However, our understanding of the fractal scattering in this ODE system was very limited. For instance, we still did not know why and under what conditions fractal scattering occurs in the system (2.6). Neither did we know many details on these fractal structures and how they depend on parameters (such as ε). This motivates us to analyze the system (2.6) in detail in this paper.

If $\varepsilon = 0$, then by defining $Y = \zeta + \mathrm{i}\psi$, (2.6) simplifies to $Y_{\tau\tau} = \mathrm{e}^Y$. Multiplying this equation by $\dot Y$ and integrating once, we find that $\dot Y^2/2 - \mathrm{e}^Y$ is a constant. Thus for the general ($\varepsilon \neq 0$) case, we define the energy E and momentum M to be the real and imaginary parts of $\dot Y^2/2 - \mathrm{e}^Y$, i.e.

$$E = \frac{1}{2}(\dot\zeta^2 - \dot\psi^2) - \mathrm{e}^\zeta \cos\psi, \tag{2.10}$$

and

$$M = \dot\zeta\dot\psi - \mathrm{e}^\zeta \sin\psi. \tag{2.11}$$

We also define

$$C = \sqrt{\frac{E + \mathrm{i}M}{2}}. \tag{2.12}$$

Then for the unperturbed system ($\varepsilon = 0$), we have

$$\frac{1}{2}\dot Y^2 - \mathrm{e}^Y = 2C^2. \tag{2.13}$$

We further introduce a quantity

$$F = -\frac{1}{C}\operatorname{acoth}\left(\frac{\dot\zeta + \mathrm{i}\dot\psi}{2C}\right) \tag{2.14}$$

which will be used in our later analysis. Here $\operatorname{acoth}(z) = \frac{1}{2}\ln\frac{x+1}{x-1}$ is the inverse hyperbolic cotangent function. In this paper, $C(\tau)$ and $F(\tau)$ need to be smooth with respect to τ. This can be achieved by piecing together appropriate branches of the multi-valued functions $\sqrt{\cdot}$ and $\operatorname{acoth}(\cdot)$ when their arguments cross over the branch cuts in the complex plane. To uniquely determine these functions, we let $\mathrm{Im}(\sqrt{\cdot}) \geq 0$ and $\mathrm{Im}(\operatorname{acoth}(\cdot)) \in [0, \pi)$ at the initial time $\tau = \tau_0$. Under these choices, functions C and F are continuous when M changes from positive values to negative ones for $E < 0$. These choices result in the formula for $\mathrm{Re}(F_0)$ given below (6.2) and the initial conditions below the map (6.11)–(6.12). More will be said on this in Section 6.

Eq. (2.6) is a two-degree-of-freedom Hamiltonian system with the conserved Hamiltonian

$$H(\zeta, \dot\zeta, \psi, \dot\psi) = E + \frac{\varepsilon}{2(1+\varepsilon)}\dot\psi^2, \tag{2.15}$$

where E is given in (2.10). Much is known concerning two-degree-of-freedom Hamiltonian systems. However, most of

those studies focused on two coupled Newtonian particles with positive masses [30–32], while the present system (2.6) depicts two coupled Newtonian particles whose masses are of different signs. Thus many previous techniques cannot be applied. In recent studies by Goodman and Haberman on approximate ODE models for strong wave interactions, Melnikov-type analysis was successfully carried out [25–28]. In those studies, the ODEs, which were also two-degree-of-freedom Hamiltonian systems, could be decoupled, with the coupling terms treated as small perturbations. Unfortunately, the present system (2.6) cannot be decoupled. Hence those methods cannot be directly applied. For (2.6), one has to work in the four-dimensional phase space at all times, and its analysis is more complex. However, we will show that the idea of Melnikov-type calculations is very helpful for the study of the present system.

In the next sections, we analyze the ODEs (2.6) in detail. Our analysis is structured as follows. In Section 3, we show for the integrable case ($\varepsilon = 0$) that solutions with $E = 0$ and $M = 0$ correspond to a one parameter family of separatrices. In Section 4, we determine the dynamics of E, M and F for the perturbed system where $\varepsilon \ll 1$. In Section 5 for the perturbed system, we analyze orbits in which a saddle approach is followed by a near separatrix orbit followed by another saddle approach. Here a saddle approach is a local minimum of ζ where separation between the two waves is largest (the reason for this name is given at the beginning of Section 5). In this way, we derive a separatrix map for E_n, M_n, and F_n at a sequence of saddle approaches. We show that the change of E_n is approximately zero. In Section 6, we simplify the map assuming $M_n/E_n \ll 1$. In this way, we obtain the simple second order separatrix map (1.1) and (1.2) for the momentum changes from one saddle approach to the next.

3. Integrable solutions and separatrix orbits

In this section, we study solutions of the integrable system (2.6) with $\varepsilon = 0$, which is needed for later analysis. Note that some of the results in this section have been obtained before in [23], but they will be reformulated here for the convenience of the present investigations. In this case, both E and M are conserved. Since (2.6) is a two-degree-of-freedom Hamiltonian system, according to Liouville's theorem, (2.6) is integrable. In the present case, we have also found a third conserved quantity. Indeed, utilizing (2.6), (2.13), (2.14) and the derivative formula $\operatorname{acoth}'(z) = 1/(1 - z^2)$, one can easily verify that $\mathrm{d}F/\mathrm{d}\tau = 1$. Hence $\operatorname{Im}(F)$ is the third conserved quantity. The analytical solution of this integrable system is [23]

$$Y(\tau) = \ln\left[2C_0^2 \operatorname{csch}^2 C_0(\tau - \tau_0 + F_0)\right], \tag{3.1}$$

where C_0 and F_0 are the initial values of C and F at $\tau = \tau_0$. Here $\operatorname{csch}(z) = 1/\sinh(z)$ is the hyperbolic cosecant function. The asymptotic behaviors of these solutions can be easily determined [23]. If we let $C_0 = a + \mathrm{i}b$, where a, b are the real and imaginary parts of C_0, then if $a \neq 0$,

$$Y(\tau) \to -2|a|\tau - \operatorname{sgn}(a)2b\tau\mathrm{i}, \quad \tau \to \infty. \tag{3.2}$$

We see that ζ escapes to $-\infty$ with exit velocity $2|a|$, and thus we call these orbits escape orbits. For these orbits, the sign of $\dot\psi_\infty$ is only determined by the sign of M since $\operatorname{sgn}(\dot\psi_\infty) = -\operatorname{sgn}(ab) = -\operatorname{sgn}(M)$. Physically, the sign of $\dot\psi_\infty$ is related to the final energy distribution between two solitary waves after interactions. If $a = 0$ but $b \neq 0$, i.e. $E < 0$ and $M = 0$, then the orbits are periodic orbits with period

$$T_p = \frac{\pi}{|b|} = \frac{\sqrt{2}\pi}{\sqrt{|E|}}. \tag{3.3}$$

If $a = b = 0$, i.e. $E = M = 0$, then the right hand side of (2.13) is zero. Integrating this first-order equation, we readily find that the solution can be written as

$$Y_s(\tau) = -\ln\left[\mathrm{i}\sigma A^{-\frac{1}{2}} + (\tau - \tau_M)/\sqrt{2}\right]^2, \tag{3.4}$$

where $A = \mathrm{e}^{\zeta_M}$, ζ_M is the maximum of ζ, τ_M is the time when $\zeta = \zeta_M$, and σ is the sign of $\dot\psi$ at $\tau = \tau_M$. This solution can also be obtained by taking $C_0 \to 0$ in Eq. (3.1). Escape orbits are unbounded, while periodic orbits are bounded. The orbits (3.4) separate the unbounded orbits from bounded ones, and hence they are called separatrix orbits. On these orbits, $\zeta \to -\infty$, $\dot\zeta \to 0$ and $\dot\psi \to 0$ as $\tau \to \pm\infty$. Notice that the separatrix orbits are not unique since ζ_M is a free parameter, and σ can be ± 1. These orbits can be regarded as a special kind of periodic orbits with $T_p = +\infty$.

The separatrix orbits above were presented through explicit formulas. It is also insightful to view these orbits in the four-dimensional phase space. First, by eliminating time from (2.10) and (2.11) with $E = M = 0$, we get $\mathrm{d}\zeta/\mathrm{d}\psi = \sin\psi/(1 - \cos\psi)$, so that an elementary integration yields an explicit one parameter family of separatrix curves,

$$2\mathrm{e}^{\zeta} = A(1 - \cos\psi), \tag{3.5}$$

where A is a positive constant (this formula can also be obtained directly from (3.4)). It is seen that when $\zeta = \zeta_M$, $\psi = (2n + 1)\pi$, where n is an integer, and hence the constant A in (3.5) is the same as the one in (3.4). When $\zeta \to -\infty$, $\psi \to 2n\pi$. We can show that $\zeta = -\infty$ and $\psi = 2n\pi$ are degenerate saddle point equilibrium points. To do so, we utilize (2.10) and (2.11) (with $E = M = 0$) as well as (3.5), and we find that

$$\dot\zeta^2 = 2\mathrm{e}^{\zeta}(1 - \mathrm{e}^{\zeta}/A). \tag{3.6}$$

This is a single well potential for ζ, with $\zeta = -\infty$ being a degenerate saddle point. Thus, the solution has the property that $\zeta \to -\infty$ as $\tau \to \pm\infty$. Similarly, we can derive the $\dot\psi^2$ equation as well, which shows that $\psi = 2n\pi$ are also saddle points. Each separatrix curve (3.5) connects an equilibrium point $\zeta = -\infty$, $\psi = 2n\pi$ to its adjacent one $\zeta = -\infty$, $\psi = 2(n \pm 1)\pi$, and thus is a heteroclinic orbit. This contrasts with separatrix curves in one degree of freedom Hamiltonian systems, which are usually homoclinic orbits connecting one saddle point $\zeta = -\infty$ to itself. The only exception occurs if $\psi = 2n\pi$ is a constant for all time τ, in which case $\zeta_M = +\infty$, and the solution develops a finite-time singularity at $\tau = \tau_M$

(see [23] and below). Such special separatrix orbits are then homoclinic orbits connecting the saddle point $\zeta = -\infty$ to itself (with a finite time singularity at $\zeta = +\infty$ in between).

We note that solution (3.1), for general values of E and M, can develop finite-time singularities for certain initial conditions. If $a \neq 0$, then the condition for singular solutions is

$$S(\tau = \tau_0) = 2k, \quad k = 0, \pm 1; \pm 2, \ldots, \tag{3.7}$$

where the function $S(\tau)$ is defined as

$$S = \frac{2|C|^2 \mathrm{Im}(F)}{\pi \mathrm{Re}(C)}. \tag{3.8}$$

If $a = 0$, the condition is $\mathrm{Im}(F_0) = 0$. These singular solutions are important, since it was observed from numerical computations that these solutions lead to fractal structures when $\varepsilon > 0$ [23]. Physically, singularities in ODEs (2.6) represent strong collisions of two solitary waves in the PDEs (2.1) (see Fig. 14 in [23]).

4. Behavior of the weakly perturbed system

From the previous section, we know that in the integrable case, the exit velocity is $2|a|$, which is a smooth function of initial conditions. Thus fractal scattering cannot occur (see Fig. 11(4) in [23] for a graph of the exit velocity function in this case). When the system is perturbed, i.e. $\varepsilon \neq 0$, however, fractal scattering appears (see Section 2 and [23]). Below, we analyze this phenomenon when $\varepsilon \ll 1$, so that the system is weakly perturbed.

In the perturbed system (2.6), most orbits escape in which case ζ approaches $-\infty$ with a non-zero exit velocity when $\tau \to \infty$ (see Fig. 2.2). For these escape orbits, we have

$$\dot{\zeta}_\infty^2 - \frac{\dot{\psi}_\infty^2}{1+\epsilon} = 2H, \qquad \dot{\zeta}_\infty \dot{\psi}_\infty = M_\infty. \tag{4.1}$$

Thus, the exit velocity $|\dot{\zeta}_\infty|$ is given by

$$|\dot{\zeta}_\infty| = \sqrt{H + \sqrt{H^2 + M_\infty^2/(1+\varepsilon)}}. \tag{4.2}$$

Since H is always conserved, to obtain $\dot{\zeta}_\infty$, we only need to know M_∞. It turns out that M_∞ is coupled to E_∞ and F_∞. To find these quantities, we first determine how M, E and F evolve with time. In the integrable case, M and E are conserved, and $\dot{F} = 1$. In the perturbed case, however, we find from (2.6) that

$$\frac{\mathrm{d}M}{\mathrm{d}\tau} = \varepsilon \mathrm{e}^{\zeta} \sin\psi \dot{\zeta}, \tag{4.3}$$

$$\frac{\mathrm{d}E}{\mathrm{d}\tau} = -\varepsilon \mathrm{e}^{\zeta} \sin\psi \dot{\psi}, \tag{4.4}$$

$$\frac{\mathrm{d}F}{\mathrm{d}\tau} = -\frac{\dot{E} + \mathrm{i}\dot{M}}{2(E + \mathrm{i}M)} F + D_1 + D_2, \tag{4.5}$$

where

$$D_1 = -\frac{(\dot{\zeta} + \mathrm{i}\dot{\psi})(\dot{E} + \mathrm{i}\dot{M})}{2\mathrm{e}^{\zeta + \mathrm{i}\psi}(E + \mathrm{i}M)}, \tag{4.6}$$

$$D_2 = 1 + \varepsilon \sin^2\psi + \mathrm{i}\varepsilon \sin\psi \cos\psi. \tag{4.7}$$

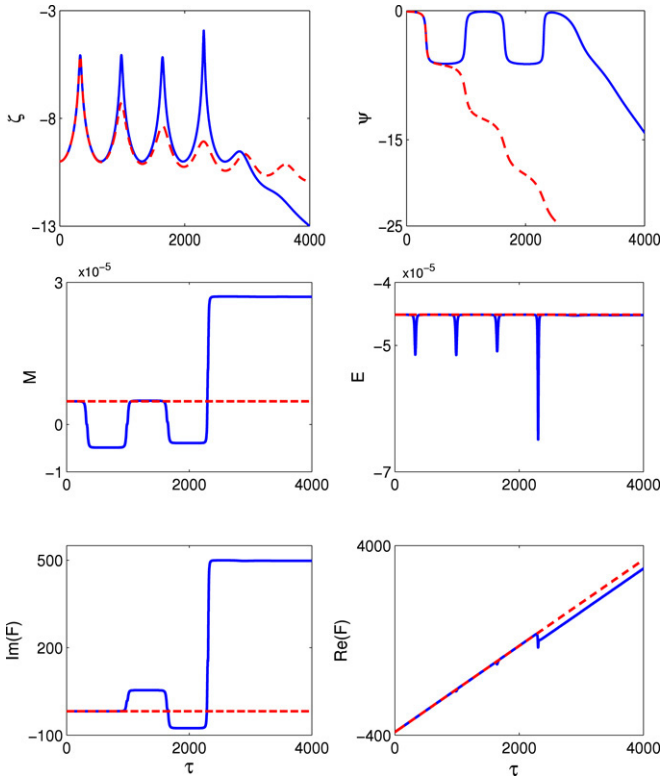

Fig. 4.1. Evolutions of ζ, ψ as well as E, M, F in the perturbed (blue solid) and unperturbed (red dashed) systems with the same initial conditions (2.8) and $\psi_0 = -0.1081$. In the perturbed system, $\varepsilon = 0.001$.

Before proceeding further, let us use a numerical example to illustrate typical solutions as well as the time evolution of (E, M, F) in order to gain some intuitive understanding and to motivate our analysis. For this purpose, we let $\varepsilon = 0.001$ and take the initial condition as (2.8) with $\psi_0 = -0.1081$, which lies in the sensitive regions of the initial-conditions space (see Fig. 2.2(a)). The time evolutions of the solutions (ζ, ψ) and quantities (E, M, F) are plotted in Fig. 4.1 (solid lines). We see that ζ undergoes five oscillations and then escapes to $-\infty$. Each oscillation corresponds to a "bouncing" motion in the two-wave interactions, similar to those found in all other physical systems exhibiting fractal scattering [10,15,18,27]. Each bounce occurs at a local maximum of ζ, where the two waves are closest and the most energy exchanges between them take place. Hence we call each ζ-maximum a bounce. After a bounce, the two waves retreat from each other, but may turn around and bounce again. Each local minimum of ζ (where separation between the two waves is largest) is called a saddle approach for reasons given in the beginning of Section 5. Saddle approaches create sensitive dependence on initial conditions, and sequences of saddle approaches (repeated bounces) lead to fractal scattering. For each orbit, we use indices $n = 0, 1, 2, \ldots$ to label its saddle-approach sequence. All variables with subscript n represent values of these variables at the nth saddle approach.

Next we examine the evolutions of E, M and F. It is seen that E and M are initially small (which holds for all weak two-wave interactions) and remain small throughout interactions. They stay roughly constant in the vicinities of saddle approaches, but undergo significant changes near

bouncing points. This is understandable, since interactions are the weakest at maximal separations (saddle approaches) and the strongest at minimal separations (bouncing points). This can also be seen from (4.3)–(4.5). From one saddle approach to the next, the net change of E is approximately zero, but the net change of M is significant and is comparable to M itself. The evolution of $\mathrm{Im}(F)$ is similar to those of M, but $\mathrm{Re}(F)$ approximately grows linearly with time since $\dot{F} = 1$ in the integrable case.

From the above observations, we see that if we have a way of determining the net change ΔM from one saddle approach to another, then we would be able to obtain the final value M_∞ after interactions, and hence ascertain the exit velocity $|\dot{\zeta}_\infty|$ from (4.2). The exact calculation of this ΔM is not possible in the perturbed system (2.6). However, it can be calculated near a separatrix asymptotically when $\varepsilon \ll 1$, which will be done in the next section.

As mentioned above, saddle approaches are important for the onset of fractal scattering. Saddle approaches are local-minimum points of ζ. The necessary and sufficient conditions for the existence of saddle approaches are that

$$\dot{\zeta} = 0, \qquad \ddot{\zeta} = \cos\psi e^{\zeta} > 0, \tag{4.8}$$

as the case of $\dot{\zeta} = \ddot{\zeta} = 0$ at a ζ-minimum cannot occur since $\zeta_{\tau\tau\tau} \neq 0$ there. Thus in view of H's definition (2.15) as well as $\varepsilon \ll 1$, the Hamiltonian H must be negative at a saddle approach. The same holds for E as well. In the next analysis, we only consider regions of initial conditions where $H < 0$. For regions with $H \geq 0$, fractal structures cannot exist.

5. The separatrix map in the perturbed system

In weak solitary wave interactions, E and M are initially small since $\zeta_0 \ll -1, \dot{\zeta}_0, \dot{\psi}_0 \ll 1$ (see (2.10) and (2.11)). Because $\varepsilon \ll 1$, E and M will remain small during later evolutions. Thus we expect the perturbed solutions in (2.6) to be near the separatrix solutions. It is known that chaotic motions often arise around separatrix orbits, and this is what happens in our system (2.6).

On the analysis of solution dynamics near separatrix orbits, some previous work is highly relevant. For weakly damped conservative systems with a linear saddle point, solutions are a large sequence of nearly homoclinic orbits (near a unique separatrix) where solutions slow down near the linear saddle point (because it is an equilibrium), pass near the saddle point, and then accelerate to follow near the unique separatrix. The points on the orbit which are closest to the saddle point are called saddle approaches. Since most of the time in the orbit is spent near a saddle point (where the motion is slow), the change in time from one saddle approach to the next can be approximated by the average period of the unperturbed periodic orbits at the energy levels of the two saddle approaches. This heuristic result can be justified more rigorously. The change in energy, on the other hand, can be approximated by using the Melnikov functions [33–35]. Similar ideas were used recently by Goodman and Haberman [25–28] for strong solitary wave interactions, where chaotic scattering occurs near a unique separatrix which connects a degenerate saddle point (at infinity) to itself. In their calculations, the change in time between two bounces (rather than between two saddle approaches) was derived by matched asymptotic expansions, while the change in energy was obtained from Melnikov functions.

For our more complicated two degree of freedom system (2.6), solutions behave similarly. The saddle point here is also at $\zeta = -\infty$. When the solution is near the separatrix, the ζ-minimum should be asymptotically near the saddle point $\zeta = -\infty$. Indeed, in the numerical example of Fig. 4.1, each local ζ-minimum is large and negative, and hence is a saddle approach asymptotically near $\zeta = -\infty$. Between two saddle approaches, there is a separatrix (3.4) with a ζ-maximum of ζ_M near which the perturbed solution lies. However, a unique feature of our system (2.6) is that (2.6) has a family of separatrices (3.4), so that ζ_M may vary from one orbit to the next (see Fig. 4.1). This differs from dynamical systems treated previously where the separatrix was always unique [25–28,33]. Due to this special feature, the determination of ζ_M in a separatrix orbit is a novel aspect in our analysis.

In this section, we asymptotically calculate the changes of M, E, F from one saddle approach to the next for (2.6) when $\varepsilon \ll 1$. The resulting map is called the separatrix map because our calculation will be performed near separatrix orbits (3.4) in view of the discussions above. In this calculation, the quantities E_n, M_n, F_n at the nth saddle approach are given, which uniquely determine this saddle approach (see (3.1)). Recall that saddle approaches exist only when $E_n < 0$. Thus in this section, E_n is required to be always negative. Our aim is to calculate these quantities at the $(n+1)$st saddle approach by integrating (4.3)–(4.5). Note that at a saddle approach, $\dot{\zeta} = 0$, and thus only three quantities, namely E, M and $\mathrm{Im}(F)$, are sufficient to characterize a saddle approach. $\mathrm{Re}(F)$ is not needed. However, we find that it is algebraically easier to work with the whole complex function F rather than just its imaginary part.

The calculations we will perform are asymptotic in the regime $\varepsilon \ll 1$, $E_n \ll 1$ and $M_n \ll 1$. Because $\varepsilon \ll 1$, the perturbed solution is close to the unperturbed solution between two adjacent saddle approaches (if they start at the same initial conditions, see Fig. 4.1). Because $E_n, M_n \ll 1$, the solutions (both perturbed and unperturbed) will be close to the separatrix solutions. The outline of our analysis is the following. We first derive changes in momentum (5.6) and energy (5.7) from one saddle approach to the next by Melnikov integrals along a separatrix (3.4). The parameters of the separatrix orbit are determined by requiring it to have the same ζ-maximum point as the unperturbed solution (3.1). It is found that the energy change is nearly zero, so that the energy at saddle approaches does not change. To find the change in F, we use the method of variation of parameters to integrate the linear inhomogeneous Eq. (4.5) from one saddle approach to the next. The time between the two saddle approaches is not simple to get in general, so we approximate it under the additional assumption that $M_n/E_n \ll 1$. In this case, the unperturbed orbit is approximately a periodic orbit with period (3.3), and this period gives the needed time.

It is noted that in the previous analysis by Goodman and Haberman on variational ODEs for strong wave interactions [25–28], the time between two saddle approaches was obtained by the matching method. That is not necessary in our case because we have explicit closed-form expressions for the unperturbed solutions which give this time directly (under our assumption). This closed-form expression of the unperturbed solution also enables us to select the appropriate separatrix orbit from its family (3.4).

In the above outline of our analysis, we made the assumption that $M_n/E_n \ll 1$. Regarding the validity of this assumption, let us look at the example in Fig. 4.1. In this case, the ratio M_n/E_n is indeed small (on the order of 0.1) before the fourth (last major) bounce. After the fourth bounce, M/E is not small. But now, M and E do not change much, so there is no need to do calculations in that region. Thus this assumption is satisfied for this example.

In more general cases, let us consider the equal initial amplitude and velocity case, where $M_0/E_0 = \tan(\psi_0)$ (see initial conditions (2.8)). In this case, it has been observed in our numerics [23] that the ψ_0-region of fractal scattering shrinks to the point $\psi_0 = 0$ as $\varepsilon \to 0$. Thus in the fractal region (which is the focus of our interest), M/E is initially small and remains small when $\varepsilon \ll 1$. In other cases (such as initial conditions (2.9)), M/E may not be small initially inside the fractal region (see Fig. 6.2). But we find that in such orbits, M/E usually does become small after the first major bounce. Thus this assumption holds at subsequent saddle approaches. If this assumption is still made for the initial saddle approach (even though it really does not hold there), our prediction for M_∞ turns out to be still very good, as Fig. 6.2 will show.

We now start our analysis by integrating (4.3)–(4.5) from one saddle approach to the next. Let us consider M first. From (4.3), we have

$$\Delta M_n = M_{n+1} - M_n = \int_{\tau_n}^{\tau_{n+1}} \varepsilon e^{\zeta} \sin\psi \dot{\zeta} \mathrm{d}\tau, \tag{5.1}$$

where τ_n and τ_{n+1} are the times of the nth and $(n+1)$st saddle approaches. Note that in previous studies by Goodman and Haberman on strong solitary wave interactions [25–28]), the discrete times $t_n, t_{n+1}, \ldots$ were chosen to be bounce times rather than saddle approaches. This needs to be kept in mind when comparing the present analysis with theirs. Since $\varepsilon \ll 1$, the perturbed solution inside the integrand will be approximated by the unperturbed solution. Thus we obtain

$$\Delta M_n = \int_{\tau_n}^{(\tau_{n+1})_u} \varepsilon e^{\zeta_u} \sin\psi_u \dot{\zeta}_u \mathrm{d}\tau, \tag{5.2}$$

which is asymptotically accurate. Here the variables with subscript 'u' represent the unperturbed solutions. Since $E_n, M_n \ll 1$, we can further approximate the unperturbed solutions in the integrand of (5.2) by separatrix solutions (3.4), and this approximation is also asymptotically accurate. Notice that separatrix orbits (3.4) are not unique, since there are three parameters σ, ζ_M and τ_M in them. We now show how to select the appropriate separatrix orbit which best approximates the unperturbed solution. We cannot ask the separatrix orbit to start at the same nth saddle approach since ζ of the separatrix orbits does not have local minima. Notice that most contributions to the integral of (5.2) come from the ζ-maximum region, thus it is natural to ask the separatrix solution to have the same ζ-maximum point as the unperturbed solution. In addition, since σ is the sign of $\dot{\psi}$ at the ζ-maximum in the separatrix orbits, it is the sign of $\dot{\psi}_u$ at the ζ-maximum. A valuable feature of our system (2.6) is that the unperturbed equations admit explicit closed-form solutions (see (3.1)). This makes it easy to implement the above requirements. These requirements uniquely determine the separatrix orbit (3.4) and lead to the following conditions,

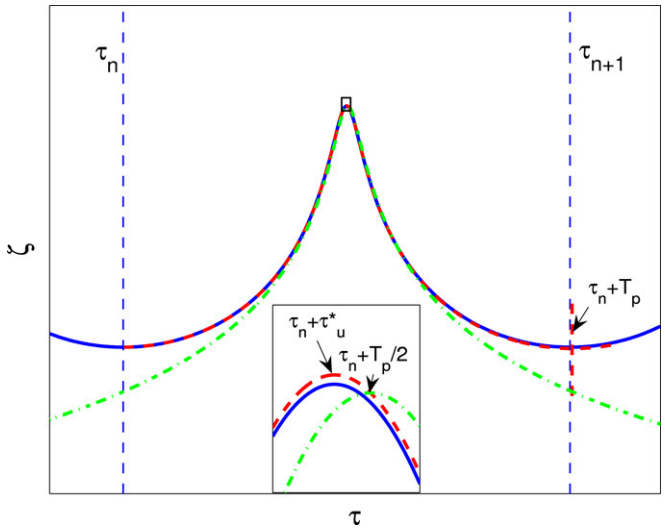

Fig. 5.1. Plots of the perturbed solution $\zeta(\tau)$ (blue solid), the unperturbed solution (red dashed), as well as the separatrix solution (green dash-dot) in our analysis. The inset is a magnification of the small box at the ζ-maximum. (For interpretation of the references to colour in this figure legend, the reader is referred to the web version of this article.)

$$\sigma_n = \mathrm{sgn}\left\{\mathrm{Im}\left[-2C_n \coth(C_n(\tau_u^* + F_n))\right]\right\}; \tag{5.3}$$

$$A_n = 2\left|C_n^2 \mathrm{csch}^2\left[C_n(\tau_u^* + F_n)\right]\right|. \tag{5.4}$$

Here $\tau_n + \tau_u^*$ is the time where ζ_u reaches its maximum. However, we still do not know τ_u^* due to the complexity of the integrable solution (3.1). This is where the assumption $M_n/E_n \ll 1$ comes in. Due to this assumption, we can expand the general solution as a series in M_n/E_n. From its leading-order term, which is a periodic solution with period (3.3), we find the leading-order approximation for τ_u^* as

$$\tau_u^* = \frac{1}{2}T_p = \frac{\pi}{\sqrt{2|E_n|}}, \tag{5.5}$$

which is asymptotically accurate when $E_n \ll 1$ and $M_n/E_n \ll 1$.

To clearly illustrate our ideas, we plot the perturbed solution, the unperturbed solution, and the separatrix solution together in Fig. 5.1. This figure was generated with typical numerical values in fractal regions, and thus is not just a schematic plot. From this figure, we see that (i) the unperturbed solution is very

close to the perturbed solution; (ii) the separatrix solution is very close to the unperturbed solution near the ζ-maximum. Away from the ζ-maximum, the separatrix orbit and the other two orbits start to deviate from each other. But in those regions, the contributions to the integral of (5.2) are negligible since ζ is large negative. Thus our separatrix-orbit approximation for the unperturbed solution is valid.

When the separatrix solution (3.4) is substituted into (5.2), we readily find that

$$\Delta M_n = \varepsilon \int_{-\infty}^{+\infty} \mathrm{e}^{\zeta_s} \sin\psi_s \dot{\zeta}_s \mathrm{d}\tau = \frac{1}{2}\varepsilon\pi\sigma_n A_n, \tag{5.6}$$

where σ_n and A_n are given by (5.3) and (5.4). Note that in the near separatrix approximation, the saddle approaches τ_n and τ_{n+1} are asymptotically large, so that τ_n and τ_{n+1} are approximated by $-\infty$ and $+\infty$ respectively in the above calculations, as is usual for Melnikov type integrals. This ΔM_n is asymptotically accurate when $\varepsilon \ll 1$, $E_n, M_n \ll 1$, and $M_n/E_n \ll 1$.

By similar calculations from (4.4) and utilizing the symmetry properties of separatrix solutions (3.4) (i.e. $\zeta_s(\tau)$ is an even function of $\tau - \tau_M$, $\dot{\psi}_s$ is even, and $\sin\psi_s$ is odd), we find that

$$\Delta E_n = \varepsilon \int_{-\infty}^{+\infty} \mathrm{e}^{\zeta_s} \sin\psi_s \dot{\psi}_s \mathrm{d}\tau = 0. \tag{5.7}$$

In other words, the energy does not change from one saddle approach to another. This is precisely what Fig. 4.1 shows. This fact is rather dramatic, and it contributes to the rather simple map we will obtain in Section 6 (see (6.11)–(6.12)).

The ΔM_n formula (5.6) depends on F_n (in view of (5.4)), and thus we also need to calculate ΔF_n in order to continue the iteration. Unlike E and M, the F equation (4.5) cannot be integrated directly over time, because the right hand side of (4.5) involves E, M and F, which can not be asymptotically approximated by such values in the unperturbed system (see Fig. 4.1). Thus different techniques must be used to calculate F_{n+1}. Here we notice that (4.5) is an inhomogeneous linear ODE for F. Recalling the definition (2.12) of C, we see that a homogeneous solution of this ODE is $F = 1/C(\tau)$. Thus by the method of variation of parameters, we find that the solution of (4.5) is

$$F(\tau) = \frac{1}{C(\tau)}\left[F_n C_n + \int_{\tau_n}^{\tau} C(s)\,[D_1(s) + D_2(s)]\,ds\right], \tag{5.8}$$

where the initial conditions $F(\tau_n) = F_n, C(\tau_n) = C_n$ have been used. Thus, the exact value of F_{n+1} is

$$F_{n+1} = F_n \frac{C_n}{C_{n+1}} + \frac{\int_{\tau_n}^{\tau_{n+1}} \sqrt{E(\tau) + \mathrm{i}M(\tau)}\,[D_1(\tau) + D_2(\tau)]\,\mathrm{d}\tau}{\sqrt{E_{n+1} + \mathrm{i}M_{n+1}}}. \tag{5.9}$$

To calculate the integral asymptotically in the above equation, note from (4.6) that

$$\int_{\tau_n}^{\tau_{n+1}} \sqrt{E + \mathrm{i}M} D_1 \mathrm{d}\tau = -\int_{\tau_n}^{\tau_{n+1}} \dot{Y}\mathrm{e}^{-Y} \frac{\dot{E} + \mathrm{i}\dot{M}}{2\sqrt{E + \mathrm{i}M}} \mathrm{d}\tau. \tag{5.10}$$

Since $E, M \ll 1$, the perturbed solution lies near the separatrix orbit (3.4) whose parameters are specified by (5.3) and (5.4). Thus we can approximate Y in the term $\dot{Y}\mathrm{e}^{-Y}$ by this separatrix solution Y_s. One may notice from Fig. 5.1 that the perturbed solution is well approximated by the separatrix solution only near the bounce point (where ζ is maximal), but not near saddle approaches. However, near saddle approaches, $(\dot{E} + \mathrm{i}\dot{M})/\sqrt{E + \mathrm{i}M} \ll 1$ since ζ is large negative (in fact, it is an exponentially small function of ζ), thus the contribution to the integral of (5.10) near saddle approaches is negligible. Hence our approximation of the perturbed solution in $\dot{Y}\mathrm{e}^{-Y}$ by the separatrix solution is justified in the whole interval $[\tau_n, \tau_{n+1}]$, and the resulting approximation to the integral in (5.10) is asymptotically accurate when $E, M \ll 1$. On the separatrix orbit, we easily see that $\dot{Y}_s \mathrm{e}^{-Y_s} = -(\hat{\tau} + \mathrm{i}\alpha)$, where $\hat{\tau} = \tau - \tau_n - T_p/2$, and $\alpha = \sigma_n\sqrt{2/A_n}$. Here the approximation (5.5) for the time of the separatrix peak has been used. Then using integration by parts, we get

$$\int_{\tau_n}^{\tau_{n+1}} \sqrt{E + \mathrm{i}M} D_1 \mathrm{d}\tau = (\hat{\tau} + \mathrm{i}\alpha)\sqrt{E + \mathrm{i}M}\Big|_{\tau_n}^{\tau_{n+1}} - \int_{\tau_n}^{\tau_{n+1}} \sqrt{E + \mathrm{i}M}\mathrm{d}\tau. \tag{5.11}$$

Regarding the D_2 integral in (5.9), recalling the expression (4.7), we see that to leading order in ε,

$$\int_{\tau_n}^{\tau_{n+1}} \sqrt{E + \mathrm{i}M} D_2 \mathrm{d}\tau = \int_{\tau_n}^{\tau_{n+1}} \sqrt{E + \mathrm{i}M}\mathrm{d}\tau. \tag{5.12}$$

Substituting (5.11) and (5.12) into (5.9), we find that

$$F_{n+1} = F_n \frac{C_n}{C_{n+1}} + \frac{(\hat{\tau} + \mathrm{i}\alpha)\sqrt{E + \mathrm{i}M}\big|_{\tau_n}^{\tau_{n+1}}}{\sqrt{E_{n+1} + \mathrm{i}M_{n+1}}}. \tag{5.13}$$

Under the assumption of $M_n/E_n \ll 1$, the unperturbed orbit can be asymptotically approximated by a periodic orbit with period T_p, where T_p is given in (3.3) with E replaced by E_n. Thus $\tau_{n+1} = \tau_n + T_p$.

Summarizing our calculations and recalling the definition (2.12) for C as well as the expressions above for $\hat{\tau}$ and α, we find that E, M and F from the nth saddle approach to the $(n+1)$st one are given by the following separatrix map,

$$E_{n+1} = E_n, \tag{5.14}$$

$$M_{n+1} = M_n + \frac{1}{2}\varepsilon\pi\sigma_n A_n, \tag{5.15}$$

$$F_{n+1} = F_n \frac{C_n}{C_{n+1}} + \frac{\pi}{\sqrt{2|E_n|}}\left(1 + \frac{C_n}{C_{n+1}}\right) + \mathrm{i}\sqrt{2}\,\sigma_n A_n^{-\frac{1}{2}}\left(1 - \frac{C_n}{C_{n+1}}\right), \tag{5.16}$$

where σ_n and A_n are given by (5.3), (5.4) and (5.5). This map was derived using the separatrix-orbit approximation as well as information on the periodic orbits of the unperturbed system. They are asymptotically accurate when $\varepsilon \ll 1$, $M_n, E_n \ll 1$, and $M_n/E_n \ll 1$.

6. Simplification of the separatrix map

The separatrix map (5.14)–(5.16) is quite complicated. It turns out that, under the same assumption $M_n/E_n \ll 1$ we have made above, this map can be greatly simplified. This will be done in this section.

Due to (5.14), $E_n = E_0$ for any n. Thus we will use E_0 to replace E_n. Next, due to the assumption $M_n/E_n \ll 1$, we can expand C_n/C_{n+1} as

$$\frac{C_n}{C_{n+1}} = 1 - \frac{M_{n+1} - M_n}{2E_0} i, \tag{6.1}$$

which is asymptotically accurate. In addition, the third term in the right hand side of (5.16) is of higher order in M_n/E_0 compared to the first two terms. Thus, to leading order in M_n/E_0,

$$F_{n+1} = F_n \left(1 - \frac{M_{n+1} - M_n}{2E_0}\mathrm{i}\right) + \frac{\pi}{\sqrt{2|E_0|}} \times \left(2 - \frac{M_{n+1} - M_n}{2E_0}\mathrm{i}\right). \tag{6.2}$$

Notice that at the first (0th) saddle approach, $\dot{\zeta}_0 = 0$, and $C_0 = \sqrt{E_0/2} + O(M_n/E_0)$. In addition, $|\dot{\psi}_0| \le \sqrt{2|E_0|}$ in view of (2.10) and (4.8). Thus from (2.14) and recalling our choices for branches of $\sqrt{\cdot}$ and $\mathrm{acoth}(\cdot)$ below (2.14), the leading-order approximation for $\mathrm{Re}(F_0)$ under the assumption $M_n/E_0 \ll 1$ is that

$$\mathrm{Re}(F_0) = -\pi/\sqrt{2|E_0|}. \tag{6.3}$$

Then the general formula for F_n can be derived as

$$F_n = \frac{\pi}{\sqrt{2|E_0|}} \left(2n - 1 - \hat{S}_n \frac{M_n}{2E_0}\mathrm{i}\right), \tag{6.4}$$

where

$$\hat{S}_{n+1} M_{n+1} = 2n M_{n+1} - (2n - \hat{S}_n) M_n. \tag{6.5}$$

This formula can be easily verified. Inserting (6.4) and (6.5) into (6.2) and neglecting second-order terms in M_n/E_0 due to the assumption $M_n/E_n \ll 1$ and (5.14), we see that (6.2) is satisfied. Notice from (6.4) that

$$\hat{S}_n = -\frac{\mathrm{Im}(F_n) 2E_0 \sqrt{2|E_0|}}{\pi M_n}. \tag{6.6}$$

Recalling the definition (3.8) for $S(\tau)$, the above expression of $\hat{S}_n$ is simply the leading-order term of $S_n = S(\tau_n)$ under the assumption $M_n/E_n \ll 1$. Thus we will treat $\hat{S}_n = S_n$ below by neglecting the higher order error.

Substituting formula (6.4) into (5.3)–(5.5) and keeping only the leading order terms with respect to M_n/E_0, we find that

$$\sigma_n = \mathrm{sgn}\left(\frac{4\sqrt{2}|E_0|}{(2n - S_n)\pi} \frac{E_0}{M_n}\right) = -\mathrm{sgn}\left[(2n - S_n) M_n\right], \tag{6.7}$$

$$A_n = \frac{16|E_0|}{(2n - S_n)^2 \pi^2} \frac{E_0^2}{M_n^2}. \tag{6.8}$$

Here we have used the asymptotic expansions of $\coth(n\pi\mathrm{i} + z) = \coth(z) \to 1/z$ and $\mathrm{csch}^2(n\pi\mathrm{i} + z) = \mathrm{csch}^2(z) \to 1/z^2$ as $z \to 0$ for any integer of n. Introducing a new variable

$$Q_n \equiv (2n - S_n) M_n, \tag{6.9}$$

then, according to (6.5), we have

$$Q_{n+1} = Q_n + 2M_{n+1}. \tag{6.10}$$

Substituting (6.7) and (6.8) into (5.15) and combining it with (6.10), we finally obtain the following simplified separatrix map,

$$M_{n+1} = M_n - \mathrm{sgn}(Q_n) \frac{8|E_0|^3 \varepsilon}{\pi Q_n^2}, \tag{6.11}$$

$$Q_{n+1} = Q_n + 2M_{n+1} \tag{6.12}$$

with initial conditions M_0 and Q_0, where $Q_0 = -S_0 M_0$ in view of (6.9). Here initial value S_0 is calculated from (3.8) and (2.14). Again, this map is asymptotically accurate when $\varepsilon \ll 1$, $M_n, E_n \ll 1$, and $M_n/E_n \ll 1$, which we have confirmed by comparing their predictions with direct numerical solutions of the ODEs.

We must emphasize that the above initial condition $Q_0 = -S_0 M_0$ is directly connected with our choices of branches for functions $\sqrt{\cdot}$ and $\mathrm{acoth}(\cdot)$ below (2.14) at the initial time. If other branches are chosen for those functions, then one can see from (2.14) that $\mathrm{Re}(F_0)$ may differ from (6.3) by a multiple of period $T_p = \pi\sqrt{2/|E_0|}$ (to the leading order in M_0/E_0), and both S_0 and $\hat{S}_0$ may change by a multiple of 2 in view of (3.8) and (6.5). Similar changes occur to F_n, S_n and $\hat{S}_n$ as well. In this case, we need to change the definition (6.9) of Q_n by an amount of a multiple of $2M_n$. This change in the definition of Q_n cancels out the change in S_n and thus leaves the value of Q_n invariant for different choices of functional branches (see (6.9)). More importantly, it would leave the separatrix map (6.11) and (6.12) invariant as well. Consequently different choices of functional branches give the same results from the map, which is to be expected. To avoid a definitional change to Q_n (and hence Q_0) associated with different choices of functional branches, our choices of branches below (2.14) are advised, in which case $Q_0 = -S_0 M_0$. Notice that our branch choices are different from those adopted by software MATLAB, where $\mathrm{Re}(\sqrt{\cdot}) \ge 0$ and $\mathrm{Im}(\mathrm{acoth}(\cdot)) \in (-\pi/2, \pi/2]$ were used. Hence if one computes the initial value Q_0 in MATLAB, two judgements are needed: (i) if $\mathrm{Im}(\sqrt{\cdot}) < 0$, then use $-\sqrt{\cdot}$; (ii) if $\mathrm{Im}(\mathrm{acoth}(\cdot)) < 0$, then use $\mathrm{acoth}(\cdot) + \pi i$.

The momentum values M_n in the above map are the key for predicting the exit velocities (see (4.2)). The quantity Q_n is an auxiliary variable, but it is very important as well. Indeed, if $Q_n = 0$, then $|M_{n+1}| = \infty$, which means that the ODE solution develops singularities right after the nth saddle approach. In the fractal structures, initial conditions for singularity solutions are the peak positions of various "hills" (see Fig. 2.2). Thus, using our map and the condition $Q_n = 0$, we can predict all the peak positions of the fractal. It is easy to show that singularities occur if and only if $S_n = 2n$ for some $n \ge 0$ (where the singularity appears right after the nth

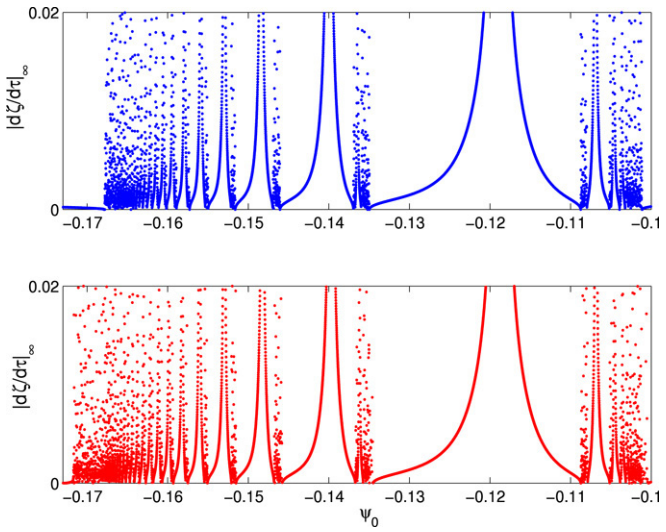

Fig. 6.1. The exit velocity ($|\dot{\zeta}_\infty|$) versus the initial phase difference (ψ_0) graphs for the initial conditions (2.8) with $\varepsilon = 0.001$. Top: from direct ODE simulations; bottom: from the separatrix map (6.11) and (6.12).

Fig. 6.2. The exit velocity ($|\dot{\zeta}_\infty|$) versus the initial phase difference (ψ_0) graphs for the initial conditions (2.9) with $\varepsilon = 0.001$. Top: from direct ODE simulations; bottom: from the separatrix map (6.11) and (6.12).

saddle approach), or initially $M_0 = 0, S_0 \neq 0$ (where the singularity appears right after the 0th saddle approach). The former condition corresponds to the singularity condition (3.7) of the integrable system, while the latter condition corresponds to the singularity condition of $\mathrm{Im}(F_0) = 0$ when $a = 0$ below (3.8).

The separatrix map (6.11)–(6.12) gives the momentum changes between two saddle approaches. In a typical ODE orbit, there are only a finite number of saddle approaches (see Fig. 4.1), but we wish to predict $M_{\tau=\infty}$. To do so, we notice that in an ODE orbit, after the last saddle approach, M quickly approaches a constant and does not change anymore (see Fig. 4.1). For the separatrix map (6.11)–(6.12), if we formally iterate them beyond the last saddle approach, we find that M_n also quickly approaches a constant, and $M_{\tau=\infty}$ is well approximated by $M_{n=\infty}$. Thus, in the text below, we will use $M_{n=\infty}$ to predict $M_{\tau=\infty}$. The validity of this approximation will be seen in Figs. 6.1 and 6.2.

In the above analysis, E_0, M_0, F_0 represent the E, M, F values at the first saddle approach. In the ODE system, we have initial conditions. If the initial conditions happen to be at the first saddle approach, i.e., $\dot{\zeta}_0 = 0$ and $\psi_0 \in (-\pi/2, \pi/2)$[the latter condition is to guarantee $\ddot{\zeta}_0 > 0$ so that ζ_0 is a local minimum, see (4.8)], then the map (6.11) and (6.12) can be iterated directly to infinity to get M_∞. In cases where the initial conditions are not at the first saddle approach, notice that from the initial time to the first saddle approach, the perturbed solution is very close to the unperturbed solution when $\varepsilon \ll 1$, and $E, M, \mathrm{Im}(F)$ are conserved in the unperturbed system. Thus, we can obtain the map's initial conditions from the initial conditions of the ODEs. This way, we can use the map (6.11) and (6.12) to predict M_∞ for general initial conditions.

Now we compare the map's predictions with numerical solutions of the ODEs (2.6). As for the PDE and ODE systems, we consider the two initial conditions (2.8) and (2.9), with ϕ_0 as the control parameter. In ODEs (2.6), we take $\varepsilon = 0.001$. For the map (6.11) and (6.12), we iterate them to infinity to get M_∞, which in turn gives $\dot{\zeta}_\infty$ from (4.2) (in practice, the map is iterated a large number of times, and the resulting M value is taken for M_∞).

First, we consider initial conditions (2.8), which is the equal-initial-amplitude case. We only need to consider the interval $\psi_0 \in (-\pi/2, \pi/2)$, where $H < 0$ (see the end of Section 4). Then all initial points in this case are saddle approaches. Using (3.8) and (2.14), we find that $S_0 = -1$ for all these initial conditions. In this case, the $|\dot{\zeta}_\infty|$ versus ψ_0 graphs from both direct ODE simulations and the separatrix map (6.11) and (6.12) are displayed together in Fig. 6.1. Due to symmetry, we only plot the chaotic regions in the left half interval $\psi_0 \in (-\pi/2, 0)$. It is seen that in the chaotic regions, $|\psi_0|$ is small, and thus M_0/E_0 is small. By comparing the map's predictions with the direct ODE values, it is clear that the map gives an accurate qualitative replication of the fractal structure in the ODEs. Even the quantitative comparison between the two shows good agreement.

Next, we consider initial conditions (2.9), which is the unequal-initial-amplitude case. In this case, $H < 0$ in the entire ψ_0 interval $(-\frac{\pi}{2}, \frac{3\pi}{2})$. The $|\dot{\zeta}_\infty|$ versus ψ_0 graphs from ODE simulations and from the map (6.11) and (6.12) are displayed together in Fig. 6.2. In this case, M_0/E_0 is not small in most parts of the ψ_0 interval, and thus assumption $M_n/E_n \ll 1$ is not met initially. In addition, the initial points are not saddle approaches in general. However, the $|\dot{\zeta}_\infty|$ graph from the separatrix map (6.11) and (6.12) still gives a very good approximation to the ODE graph both qualitatively and quantitatively. The reason for this has been given in the last section. These excellent agreements between the map's predictions and ODE solutions show that the map (6.11) and (6.12) is a very valuable tool for the understanding of fractal scattering in weak two-wave interactions.